International Journal of Advances in Engineering and Management (IJAEM)
Volume 5, Issue 2 Feb. 2023, pp: 310-320 www.ijaem.net ISSN: 2395-5252

"Application of Solar Chimney in Building Ventilation: An Approach to Green Energy Building"

Ms. Roshni Ningthoujam, Prof. Abhay Shelar, Prof. Sagar Gawande

M.E (Environment Engineering)Department of Civil Engineering APCOER, Pune-46
Head of Deoartment (Environment Engineering)Department of Environment Engineering APCOER, Pune-46
P.G Co-Ordinator (Environment Engineering) APCOER, Pune-46

Date of Submission: 01-02-2023 Date of Acceptance: 10-02-2023

ABSTRACT
The global interest in solar energy as an alternative to traditional fuels has led to a significant overall increase of attentiveness to solar energy systems, especially the solar chimney system. Because one potential drawback of solar chimney systems is the low efficiency of more traditional solar chimneys, researchers and scientists are trying to improve the efficiency of the solar chimney system by integrating them with other conventional or renewable energy systems called hybrid solar chimneys. The current review article examines solar chimney systems combined with other renewable or conventional energy systems. The emphasis of this article was placed on inclined solar chimneys with geothermal energy with two different settings. These hybrid solar chimney have shown improved efficiency in improvement of ventilation as described in this paper. Suggestions and future scope have been suggested to improve the hybrid solar chimney

Keywords— Inclined solar chimney; Green Building, geothermal energy, Ventilation, ANSYS, Computational fluid dynamics

I. INTRODUCTION

Green buildings minimize energy and water use and are a vital element of sustainable urban development that attempts to counteract climate change. Below, we examine a few green structures which pave the way for more responsible urban development, ranging from massive skyscrapers to innovative museums.The United Nations (UN) estimates that in 2050, about 68 percent of people would reside in cities. They only make up 3 percent of surface of the world, but they account for 60 percent of greenhouse gas emissions and 78percent of energy use. Because of this, UN improved New Urban Agenda in 2016 to provide guidance to nations on their urbanization efforts and create cities that are more livable, healthy, inclusive, sustainable, and resilient. Iberdrola is a part of Association of Madrid World Capital of Engineering and Architecture (MWCC). This organization promotes these industries in nation's capital as well as throughout rest of Spain, reinforcing dominance of Spanish businesses on global market and establishing Madrid and Spain as a global reference hub for urban solutions.New urban planning trends involve the creation of eco-neighborhoods, as opposed to commuter towns which sprang up as an outcome of Industrial Revolution and develop mentalism of 20th century. These eco- neighborhoods are urban projects with dual goals of minimizing their negative impact on the environment and encouraging residents to adopt more environmentally friendly lifestyles. Utilizing sustainable technology and materials in development of buildings and other infrastructures is essential to this kind of project. A green or sustainable structure is one that, by its construction and features, maintains or raises the local quality of life. To do this, it is necessary to reach a high level of efficiency: decreasing utilize of water, energy, and other resources minimizes environmental damage. (Leadership in Energy and Environmental Design) LEED certification is worldwide recognized formal designation which determines if a building deserves to be called sustainable.

II. NATURAL VENTILATION IN BUILDING

The majority of older buildings had some form of natural ventilation, however many of

International Journal of Advances in Engineering and Management (IJAEM)
Volume 5, Issue 2 Feb. 2023, pp: 310-320 www.ijaem.net ISSN: 2395-5252

these structures' ventilation systems have since been degraded due to installation of partition walls and mechanical devices. Natural ventilation, as opposed to more commonpractice of using mechanical ventilation, is gaining popularity as a means of reducing energy consumption and expenses, ensuring adequate indoor environmental quality, and keeping an indoor climate that is healthy, comfortable, and conducive to productive activity. This is because there is a growing understanding of costs and environmental effects of energy usage. In buildings with the correct climate and construction, natural ventilation can replace air conditioning systems resulting in 10 to 30% decrease in total energy use. Fresh air is circulated through a building using pressure differentials in a naturally ventilated system. Wind or buoyancy impact induced by temperature or humidity changes can also cause a noticeable change in atmospheric pressure. In any case, the amount of ventilation will be significantly influenced by the size and location of building's openings. It is helpful to think of a natural ventilation system as a circuit that values both supply and exhaust air equally. Transom windows, louvers, grilles, and open floor layouts are methods for completing airflow circuits throughout a building (figure 1.2). When designing a system that relies on natural ventilation, the architect often runs into challenges when trying to meet code requirements for how smoke and fire should be transmitted. For instance, many code regulations now prohibit use of staircases as exhaust stacks, which was common in historic buildings. Instead than using mechanical fans, wind and buoyancy are harnessed to bring in fresh air in natural ventilation systems. Recirculating fresh air is essential for odor control, human health (oxygen), and thermal comfort in buildings. 160 feet per minute (fpm) air velocity can cause a 5 °F reduction in the interior's perceived temperature. Natural ventilation, in contrast to conventional air conditioning, is not very good at lowering the relative humidity of air that is brought in. Because of this, use of natural ventilation is restricted in regions with high humidity.

1. GEOTHERMAL SYSTEMS

When temperature of ground is higher than surrounding air, heat can be transferred from ground to the structure using a heat pump. A net energy benefit can be achieved as a result of use of the heat pump because it can extract up to five times as much energy from ground than is required to power system. If the heat pump is reversed, it can be used to eliminate heat from an interior environment by releasing it into earth. To operate, ground-source heat pumps' heating & cooling functions need only a modest quantity of electricity. Users of geothermal heat pumps should be mindful that these systems might not be completely fossil fuel free if they are not paired with renewable electricity to power cooling and heating process (e.g., modes) (e.g., renewable-based).

2. Computational Fluid Dynamics

The Dynamics of Computational Fluid is the modeling (mathematical physical problem formulation) simulation of fluid engineering systems and computational approaches (solvers, grids generations, discretization methods & numerical parameters, etc.)

The Naviers-Stokes equation is founded on momentum, mass, and energy conservation. The equations include momentum, continuity, and energy equations.

Energy equation

Continuity equation.

$$\frac{Dp}{Dt} + \frac{\rho \partial U}{\partial x} = 0$$

Momentum equation

$$\frac{\rho \partial U}{\partial t} + \frac{\partial U}{\partial x} = -\frac{\partial P}{\partial x} - \frac{\partial \tau}{\partial x} + \rho g$$

Energy equation

$$\frac{\rho c \partial T}{\partial t} + \frac{\rho c U \partial T}{\partial x} = -\frac{P \partial U}{\partial x} + \frac{\lambda \partial T}{\partial x 2} - \frac{\tau \partial U}{\partial x}$$

General form of Navis-Stokes equation

As a means of simplifying the Navier-Stokes equatios, we could alter them.

$$\frac{\partial(\rho\phi)}{\partial t} + \partial/\partial x(\rho U\phi - \partial\emptyset/\partial x) = q$$

Problem Definition

With the increase in energy demands owing to

International Journal of Advances in Engineering and Management (IJAEM)
Volume 5, Issue 2 Feb. 2023, pp: 310-320 www.ijaem.net ISSN: 2395-5252

growing population and urbanization, there arises the need for a renewable source of energy which can be effectively used for cooling and ventilation purpose of buildings. Inclined solar chimney application is in initial research phase and requires further investigation to provide cooling or heating effect usinggeothermal mechanisms.

III. AIM

The goal of the current effort is to simulate airflow via a solar roof Chimney in two dimensions. A length is specified for the inlet and outflow.

IV. OBJECTIVES

This study's objective is to add perforated plate into design of a geothermal mechanism and solar chimney in order to examine its impact on ventilation.

- Building CAD model of room of size 1m*1m*1m.
- Performing cfd analysis using ANSYS CFX.
- Taking air inlet from ground(geothermal excahnge)
- Incorporating geothermal mechanism to get cooling effect (1st design configuration)
- Incorporating geothermal mechanism to get cooling effect (2nd design configuration)
- Comparative analysis of inclined solar chimney (generic design) and with new design of solar chimney (with geothermal mechanism)

V. COMPUTATIONAL DOMAIN

a computational domain with a 1m length and 1m width, with a 0.35m inlet (suction) opening on the right wall and a 0.35m outlet hole in the ceiling above. As can be seen in Figure 5.1 below, the computational domain of the chimney is represented within CREO design program for inclined solar chimneys.

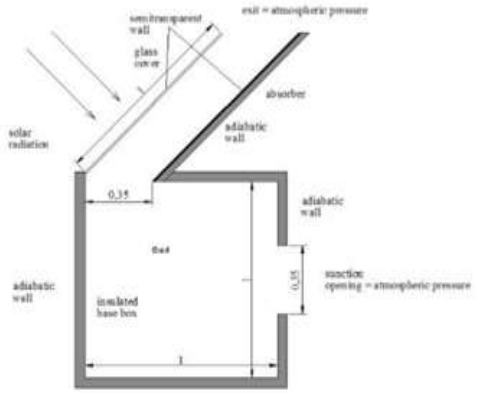

Fig 5.1: Schematic of inclined solar chimney

Meshing

Fine sizing and brick elements are employed to create model's mesh. The growth rate is targeted to 1.2 percent, inflation is normal, and there are five tiers. The meshed model of computational domain

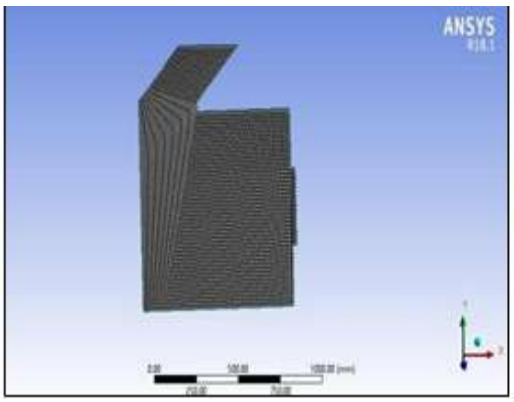

Fig 5.2: Meshing of inclined chimney

ANSYS meshes are used to create the mesh for vertical chimney. Here, brick-shaped elements are assumed to have a fine size and 100-percent-relevant weighting. As shown in fig.5.2, further meshing settings, including smoothing, transition, and curvature angle is set to medium, slow, and 120.

Relevance Center	Fine
Initial Size Seed	Active Assembly
Smoothing	Medium
Transition	Slow
Span Angle Center	Fine
Curvature Normal A...	Default (12.0 °)
Min Size	Default (1.4214e-004 m)
Max Face Size	Default (1.4214e-002 m)
Max Size	Default (2.8429e-002 m)
Growth Rate	Default (1.10)
Minimum Edge Length	5.e-003 m

Fig. 5.3: Meshing Parameter

Meshing

The domain is considered to be fluid in nature. The domain is considered to be fluid in nature. In this investigation, a two- variable k-epsilon turbulence model has been built up, and the inlet velocity has been altered. Fluid is regarded as air. The radiation model has been established. Various domains i.e. absorber plate, glass, insulation are defined. It is defined that for air domain there is an air outlet, an air inlet, and a symmetry boundary condition.

International Journal of Advances in Engineering and Management (IJAEM)
Volume 5, Issue 2 Feb. 2023, pp: 310-320 www.ijaem.net ISSN: 2395-5252

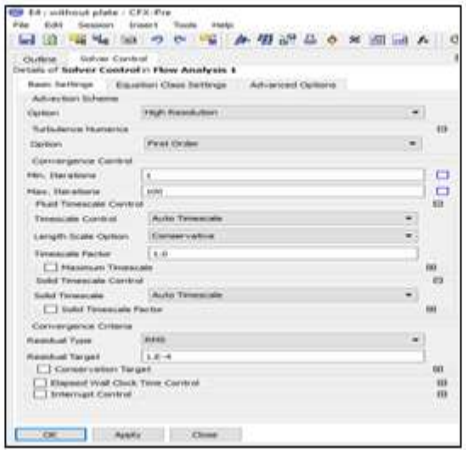

Fig 5.4: Convergence settings

Solution

The solution controls involve setting RMS residual values to
.0001 and number of iterations set to 100. The 2nd order upwind scheme is selected for the simulation.

VI. RESULT & DISCUSSION

ANSYS CFX software was used to conduct the analysis, which compared two versions of an inclined solar chimney: one without a geothermal design mechanism and another with such a mechanism. There are 2 different geothermal layouts put into use. The first design is without any roughness (smooth tube) and 2nd design is with artificial roughness.

Inclined solar chimney without geothermal mechanism

This section describes the results obtained from CFD analysis for inclines solar chimneys without any geothermal mechanism.

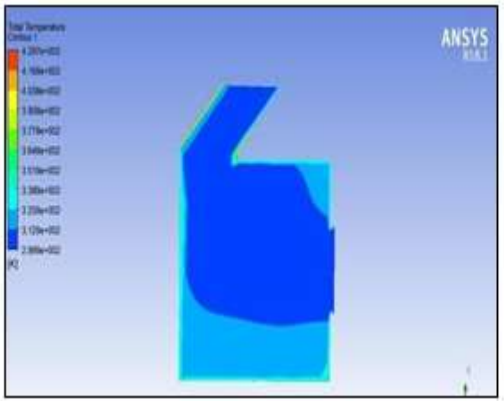

Fig 6.1: Temperature plot for inclined solar chimney without perforated plate

Figure 6.1 provides a representation of the temperature plot that was derived from the CFD analysis. The plot reveals that the temperature was greater in the area close to glass and absorber plate. Radiation disperses the heat throughout the domain, causing it to be felt in other locations. Monte Carlo analysis is performed using a multiband spectral radiation model. It's warmer towards the room's edges than it is in the middle. This is because of air movement, which results in convective heat transfer, in dark blue areas

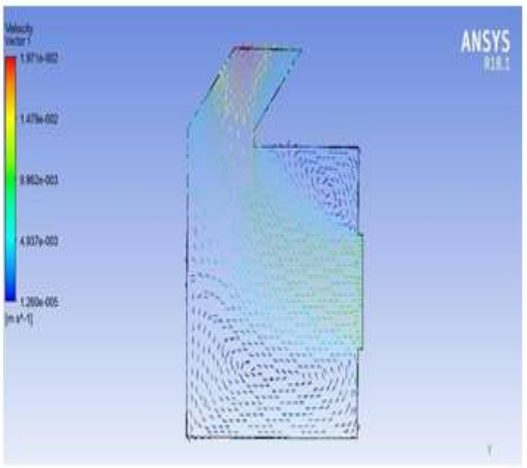

Fig 6.2:Velocity vector for inclined solar chimney without perforated plate

above illustrates the velocity vector plot. The graph depicts vortex creation in two places. The first zone is located in lower left area, while second region is located in upper right area. The zone where air flows directly from the entrance to the outlet has greatest convective heat transfer. As depicted in Figure 6.1, this type of air flow results in vortex zones with greater temperatures.

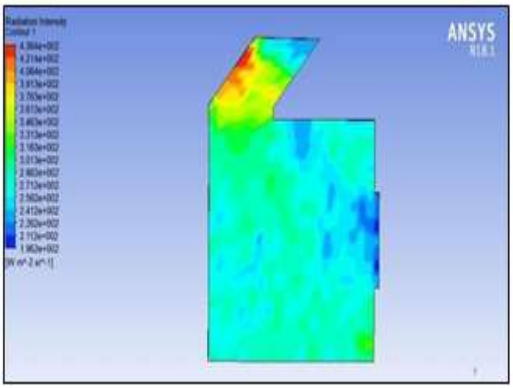

Fig 6.3: Radiation intensity of inclined solar chimney

International Journal of Advances in Engineering and Management (IJAEM)
Volume 5, Issue 2 Feb. 2023, pp: 310-320 www.ijaem.net ISSN: 2395-5252

Figure 6.3 above displays the radiation intensity plot. As a result of path of incident radiation, regions close to incidence glass surface and lower right area of graph exhibit a greater intensity of 436.4 W/m2 sr.

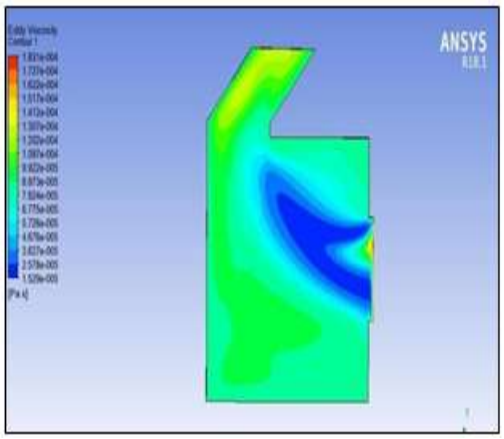

Fig 6.4: Eddy viscosity for inclined solar chimney without perforated plate

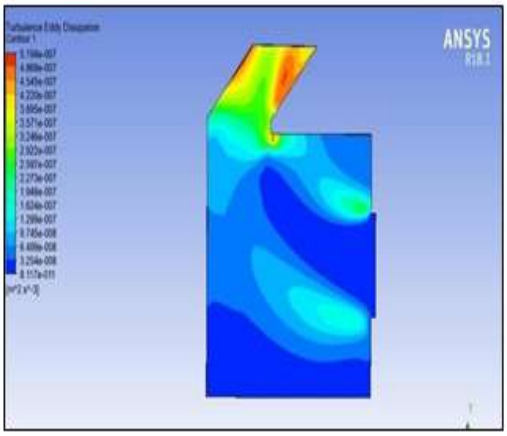

Fig 6.5: Turbulence eddy dissipation for inclined solar chimneywithout perforated plate.

Areas with straight air flow vectors (without swirl) have lower temperatures than those with swirling or turbulence-producing air flow vectors. The same is evident from eddy

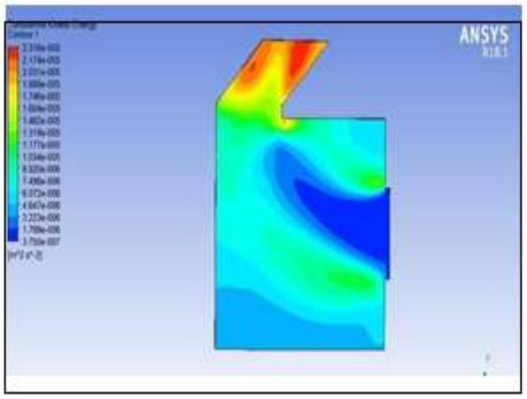

Fig 6.6: Turbulence kinetic energy for inclined solar chimney without perforated plate

The regions that are nearest to exit and those that are immediately surrounding absorber glass and plate surface on which sunlight is incident have highest levels of kinetic energy which is caused by turbulence. Figure 6.7 below illustrates the pressure graph. Negative pressure (suction) is observed between glass (where sun's rays are incident) and absorber plate in pressure plot.

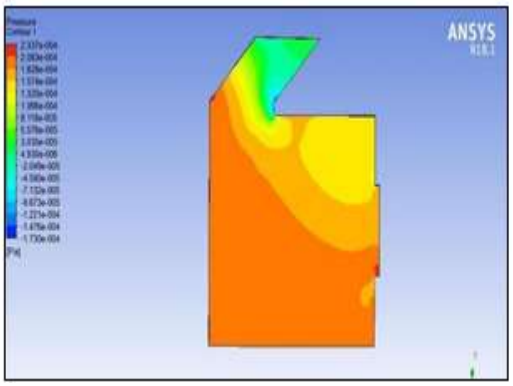

Fig 6.7: Pressure contour for inclined solar chimney without perforated plate

The negative pressure is shown by light blue and dark blue colored regions as shown in figure 6.7 above. The other regions of the room at bottom and near the opening show positive pressure. The negative pressure on the top between glass and absorber plate and positive pressure on other locations results in air flow from positive pressure region to negative pressure region. This is evident from vector plot as shown in figure 6.2.

Geothermal Design configuration 1

Further analysis is conducted using geothermal mechanism combined with inclined solar chimney as shown below. The dimensions are shown below. The depth is 2284 mm from window level and

International Journal of Advances in Engineering and Management (IJAEM)
Volume 5, Issue 2 Feb. 2023, pp: 310-320 www.ijaem.net ISSN: 2395-5252

length is 3558mm.

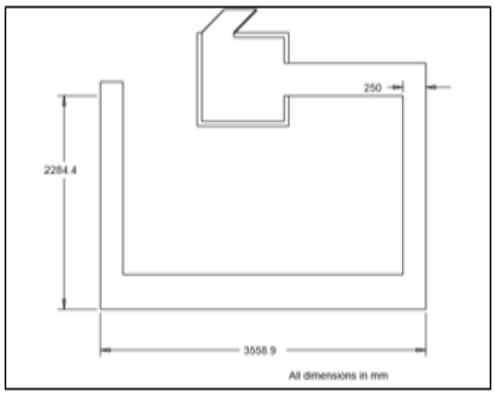

Figure 6.8: Dimensions of geothermal configuration 1

CFD analysis is conducted using geothermal mechanism as shown below. Figure 6.9 shows the air intake and exhaust as well as symmetric boundary conditions.

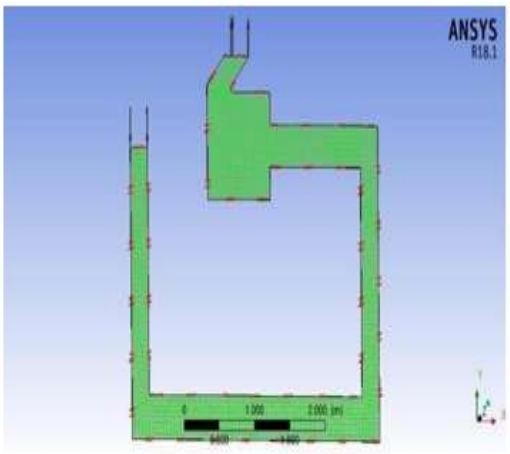

Figure 6.9: Loads and boundary condition on geothermal design configuration 1

The air inlet is made through top left face of geothermal pipe as shown above with temperature of 295K and velocity of .01 m/s. The outlet is on top face of inclined solar chimney, the stacking effect is generated due to solar radiation incident on plate which reduces pressure and in turn sucks air from outside. The temperature on the walls of geothermal tube is setto 295K.

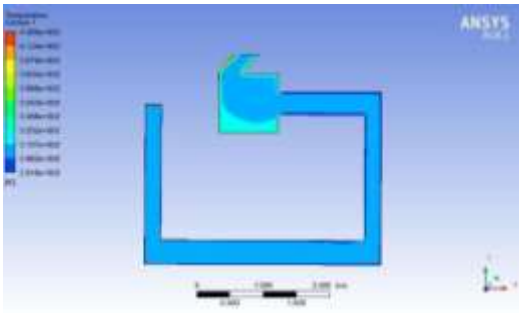

Figure 6.10: Temperature plot of geothermal mechanism Figure 6.10 depicts the temperature distribution of ageothermal mechanism with a inclined chimney. In majority of geothermal tube locations, temperature plot demonstrates a consistent magnitude. Lower temperature, magnitude 297K, is present in airflow zone. The areas where the air swirls, i.e. bottom left area, have temperatures close to 310.7K.

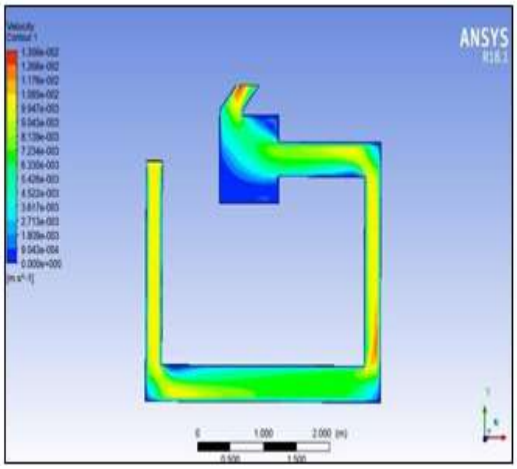

Figure 6.11: Velocity plot of geothermal mechanism

Above, in Figure 6.11, is a plot of velocity. The yellow area of plot represents the area where the air velocity is relatively constant for the left-end tube. The green area represents the range of velocities along the horizontal tube. For right-hand tube, the velocity value is practically constant; it decreases as tube advances inside room, but then increases as it nears the exit.

International Journal of Advances in Engineering and Management (IJAEM)
Volume 5, Issue 2 Feb. 2023, pp: 310-320 www.ijaem.net ISSN: 2395-5252

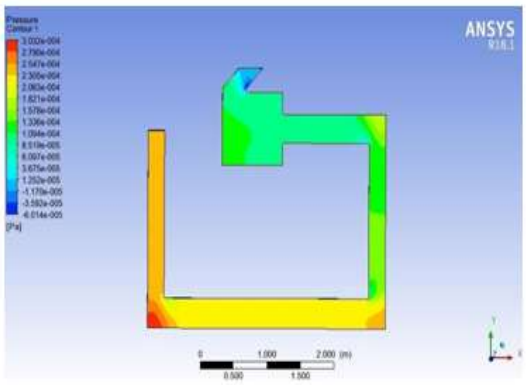

Figure 6.12: Pressure plot of geothermal mechanism

The pressure plot shows positive pressure (compressive) on almost all the regions of geothermal tube and on regions inside room. The zone near glass and absorber plate has shown negative pressure which results in suction and air flows from high pressure to low pressure as shown in figure 6.13 below.

Figure 6.13: Velocity vector plot

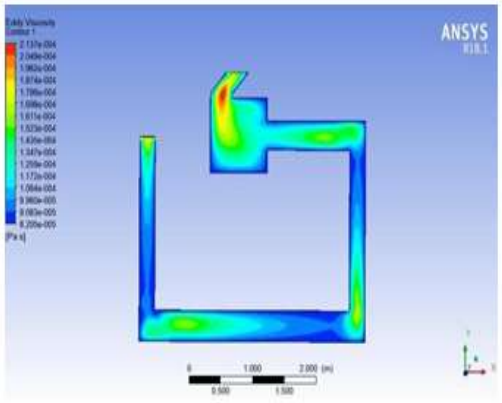

Figure 6.14: Eddy viscosity plot of geothermal mechanism

The plot of eddy viscosity is depicted in figure 6.14. The plot shows higher eddy viscosity between glass and absorber plate and on some regions of geothermal tube. The maximum eddy viscosity zone can be corroborated with vector plot as shownin figure 6.13 above.

Geothermal Design configuration 2

Further analysis is conducted using geothermal design 2 with artificial roughness combined with inclined solar chimney as shown below. The imported CAD model is shown below. The depth is 2284 mm from window level and length is 3558mm.

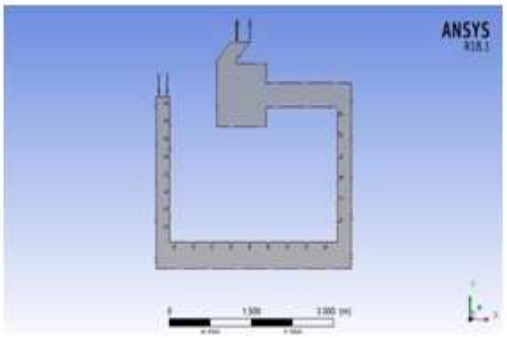

Figure 6.15: Imported CAD model of geothermal designconfiguration 2

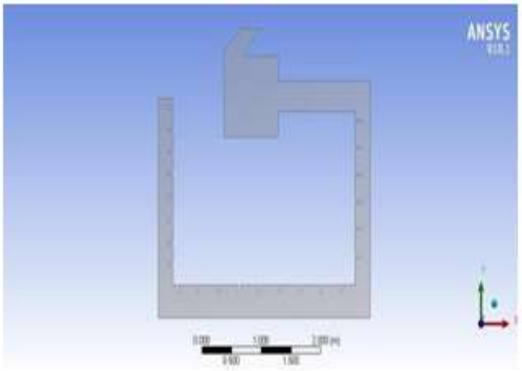

Figure 6.16: Eddy viscosity plot of geothermal mechanism

CFD analysis is conducted using geothermal mechanism as shown in figure 6.15 above. Figure 6.16 above depicts the air entrance, air outflow, and boundary condition for symmetry. The air inlet is made through top left face of geothermal pipe as shown above with temperature of 295K and velocity of .01 m/s. The outlet is on top face of inclined solar chimney, the stacking effect is generated due to solar radiation incident on plate which reduces pressure and in turn sucks air from outside. The temperature on the walls of geothermal tube is set to 295K.

International Journal of Advances in Engineering and Management (IJAEM)
Volume 5, Issue 2 Feb. 2023, pp: 310-320 www.ijaem.net ISSN: 2395-5252

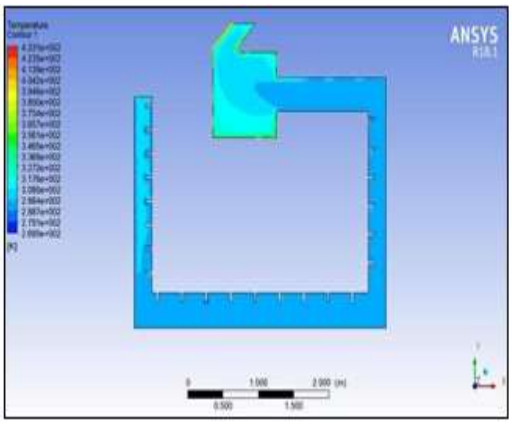

Figure 6.17: Temperature plot of geothermal mechanism

Above, in Figure 6.17, is a temperature profile of a geothermal mechanism with an inclination chimney. For the most part, geothermal tube's temperature has remained quite stable, as depicted by plot. The air flow zone has a temperature 297K lower than the surrounding area. The temperature in bottom left section, where the air is swirling, is close to 308K.

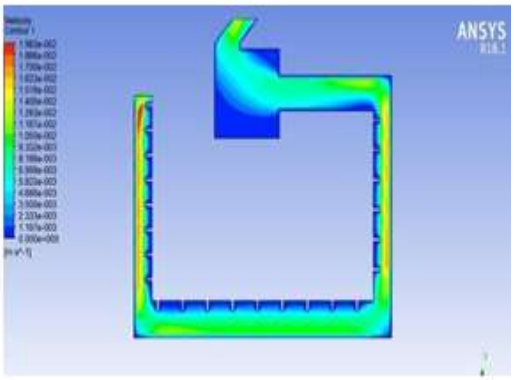

Figure 6.18: Velocity plot of geothermal mechanism

Figure 6.18 displays the velocity graph. Figure 6.18 displays the velocity graph. The red area of plot indicates an area with higher air velocities, where the artificial roughness is either first or second order. As we continue to descend the left tube, speed gradually lowers. As green zone indicates, the bottom of the structure experiences the highest air velocities. As dark blue area illustrates, the space between roughness and bottom left and top right areas is where speed is slowest.

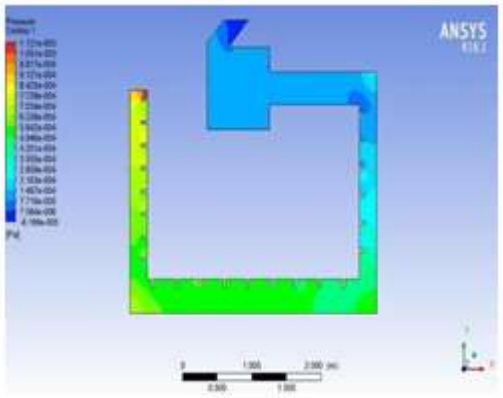

Figure 6.19: Pressure plot of geothermal mechanism

The pressure plot shows positive pressure (compressive) on almost all the regions of geothermal tube and on regions inside room and on zones of left, bottom, and side tube of geothermal mechanism. The zone near glass and absorber plate has shown negative pressure which results in suction and air flows from high pressure to low pressure. The variation in air pressure is much high across length of bottom tube and on left/right tubes as shown by green and light blue colored zones.

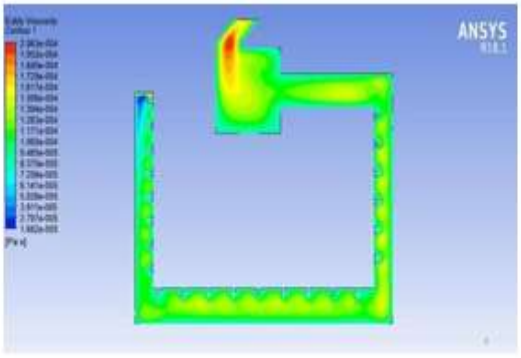

Figure 6.20: Eddy viscosity plot

The eddy viscosity plot is shown in figure 6.20 above. The plot shows higher eddy viscosity between glass and absorber plate and on some regions of geothermal tube. The eddy viscosity has lowest magnitude near air inlet.

Geometry Details	Inlet Temp (K)	Outlet Temp(K)	Temperature Difference (K)	Average temperature (K)
Without geothermal	300	310.33	10.33	309.69
With geothermal design 1	295	310.67	15.67	300.41
With geothermal design 2	295	311.16	16.16	299.42

International Journal of Advances in Engineering and Management (IJAEM)
Volume 5, Issue 2 Feb. 2023, pp: 310-320 www.ijaem.net ISSN: 2395-5252

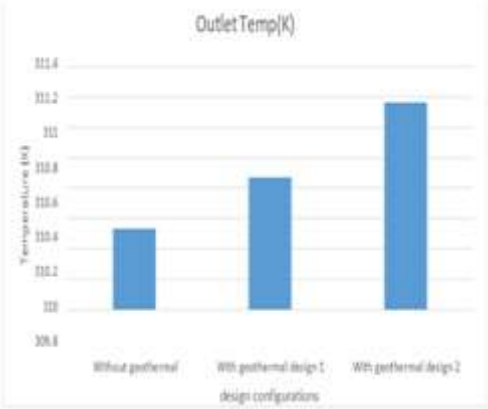

Figure 6.17: Outlet Temperature graph

The outlet temperature comparison plot shows almost similar outlet temperatures for all the three-design configurations i.e. (310K to 311K). Geothermal design 2 has slightly higher temperature as compared to other 2 design configurations.

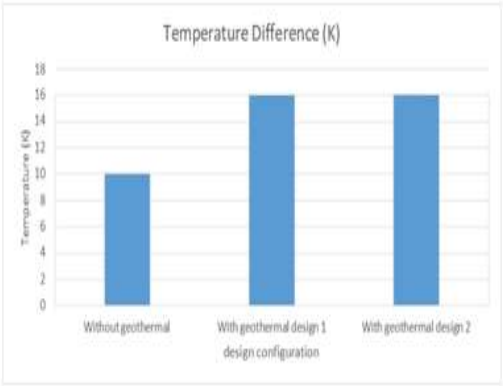

Figure 6.17: Temperature Difference

The comparison of the temperature differences is depicted in plot that can be found above in figure 6.22. The graph demonstrates a greater temperature difference for geothermal design2, which is then followed by geothermal design1, and generic design demonstrates temperature difference that is smallest (without geothermal).

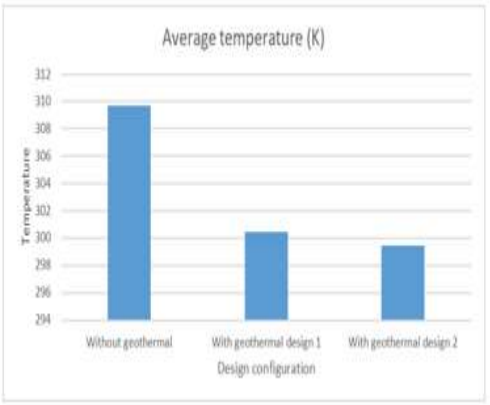

Figure 6.17: Average temperature of 3 design configurations

The average temperature comparison plot for all the 3-design configurations is shown in figure 6.23 above. The maximum average temperature of room is observed for design without any geothermal mechanism as shown by 1st bar with temperature nearly 309K. the minimum average temperature is observed for geothermal design 2 with average room temperature nearly 299.4K.

Geometry Details	Static Enthalpy (J/Kg)	Average Mass Flow (Kg/s) * 10^{-3}
Without geothermal	11591	8.23488
With geothermal design 1	2277	5.78872
With geothermal design 2	1284	5.78872

Table 6.2: Enthalpy and average mass flow

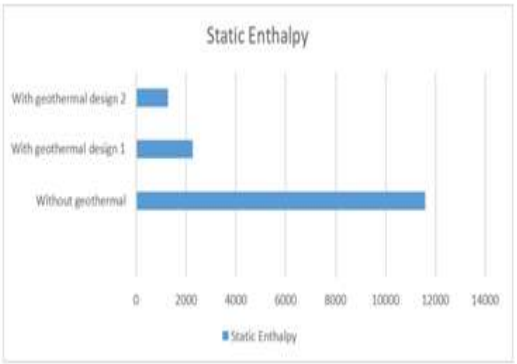

Figure 6.24: Static enthalpy of 3 design configuration

The plot of static enthalpy is displayed up there in figure 6.24. The enthalpy represents the energy stored in fluid due to temperature and pressure. The maximum static enthalpy is observed for generic design (without any geothermal mechanism) and minimum enthalpyis observed for geothermal design 2. Due to greater temperatures and a smaller temperature difference between outlet and inlet, generic designs have a higher enthalpy. The higher enthalpy results in higher heating of

International Journal of Advances in Engineering and Management (IJAEM)
Volume 5, Issue 2 Feb. 2023, pp: 310-320 www.ijaem.net ISSN: 2395-5252

room.

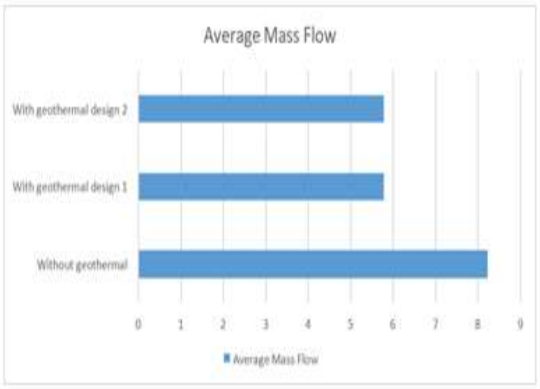

Figure 6.25: Average mass flow of 3 design configuration

The average mass flow for 3 design configurations is shown in figure 6.25 above. The increased temperature difference (resulting in higher cooling of room) in geothermal designs caused penalty in mass flow and thus reduced ventilation. The mass flow is almost same for both geothermal design configurations.

The heat extraction is given by the following formula

$Q=m*c*\Delta T$

Where

M is mass flow rate

C is specific heat capacity of air i.e. 1004.4 J/Kg K

ΔT is temperature difference

Geometry Details	Average Mass Flow (Kg/s) * 10^{-5}	Temperature Difference (K)	Heat extracted (Joules)
Without geothermal	8.23488	10.33	.854
With geothermal design 1	5.78872	15.67	.911
With geothermal design 2	5.78872	16.16	.939

Table 6.3: Heat extracted

Figure 6.26 below compares the efficiency of heat extraction in three distinct layouts. Heat extraction is found to be highest for Geothermal Design2, then Geothermal Design2, and lowest for Generic Design in comparison graph.

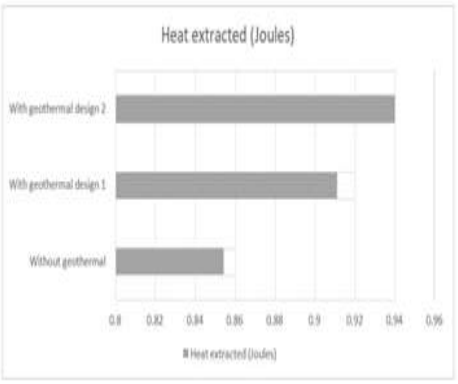

Figure 6.26: Heat extraction comparison

VII. CONCLUSION

For both designs with and without a geothermal mechanism, ANSYS CFX is used to do a CFD analysis of solar chimneys. Radiation levels, average air velocity, and temperature are all measured and analyzed.

1. The average radiation intensity in room decreases moving away from left glass on which solar radiation is incident. The radiation on central region of room is minimum.
2. The lowest average temperature of room is observed for geothermal design 3 with magnitude of nearly 299K.
3. The highest average temperature of room is observed for generic design (without geothermal mechanism) with magnitude of nearly 309.69K.
4. By using a geothermal mechanism, the mass flow rate can be decreased. Despite this, cooling effect is superior to that of a standard layout.
5. It is best to use a geothermal design3, while a generic design will provide the least amount of cooling.
6. Geothermal design 3 achieves best in-room cooling, whereas generic design achieves least.
7. The heat transfer rate using geothermal mechanism is nearly .93J and without any geothermal mechanism (generic design) is 854J.
8. For general designs, enthalpy is maximum, whereas, for geothermal designs, it is lowest.

Future Scope

The application of inclined solar chimney can be contemplated for commercial buildings like hospitals, muti-storied buildings which invites further research using experimental and simulation techniques.

REFERENCES

[1] Yang, G.; Shi, H.; Xu, D.; Shen, Z.; Zhang, Z.; Shen, H.; Wang, Z. Research on simulation of energy consumption of ground water-source heat pump air conditioning system in plant factory. IOP Conf. Ser. Earth Environ. Sci. 2021, 770, 012044. [CrossRef]

[2] Fernández, J.C.R. Integration capacity of geothermal energy in supermarkets through case analysis. Sustain. Energy Technol. Assess. 2019, 34,49–50. [CrossRef]

[3] Cadelano, G.; Cicolin, F.; Emmi, G.; Mezzasalma, G.; Poletto, D.; Galgaro, A.; Bernardi, A. Improving the energy efficiency, limiting costs and reducing CO2 emissions of a museum using geothermal energy and energy management policies. Energies 2019, 12, 3192. [CrossRef]

[4] Bisoniya, T.S. Design of earth–air heat exchanger system. Geotherm. Energy 2015, 3, 18. [CrossRef]

[5] Bisoniya, T.S.; Kumar, A.; Baredar, P. Study on Calculation Models of Earth-Air Heat Exchanger Systems. J. Energy 2014, 2014, 1–15. [CrossRef]

[6] Rodrigues, M.K.; Vaz, J.; Rocha, L.A.O.; Santos, E.D.d.; Isoldi, L.A. A full approach to Earth-Air Heat Exchanger employing computational modeling, performance analysis and geometric evaluation. Renew. Energy 2022, 191, 535–556. [CrossRef]

[7] Mathur, A.; Kumar, S. Thermal performance and comfort assessment of U-shape and helical shape earth-air heat exchanger in India. Energy Built Environ. 2022, 3, 171–

[8] 180. [CrossRef]

[9] Benhammou, M.; Sahli, Y.; Moungar, H. Investigation of the impact of pipe geometric form on earth-to-air heat exchanger performance using Complex Finite Fourier Transform analysis. Part I: Operation in cooling mode. Int. J. Therm. Sci. 2022, 177, 107484. [CrossRef]

[10] Guo, X.; Wei, H.; He, X.; Du, J.; Yang, D. Experimental evaluation of earth–to–air heat exchanger and air source heat pump hybrid indoor air conditioning system. Energy Build. 2022, 256, 111752. [CrossRef]